สำนักงานคณะกรรมการการอุดมศึกษา
กระทรวงศึกษาธิการ
http://www.mua.go.th

รายงานวิจัยฉบับสมบูรณ์

โครงการ: การศึกษามอร์ฟอร์จีนีสิสโดยอาศัยวิธีฟิสิกส์เชิงสถิติ การสร้างแบบจำลองทางคณิตศาสตร์ และการทดลองเชิงคอมพิวเตอร์

The studies of Morphogenesis by using Statistical Physics, Mathematical Modeling and Computer Simulations

โดย ผศ. ดร. วรรณพงษ์ เตรียมโพธิ์

มิถุนายน พ.ศ. 2547

สัญญาเลขที่ TRG4580090

รายงานวิจัยฉบับสมบูรณ์

โครงการ (ภาษาไทย): **การศึกษามอร์ฟอร์จีนีสิสโดยอาศัยวิธี ฟิสิกส์เชิงสถิติ การสร้าง แบบจำลอง คณิตศาสตร์ และการทดลองเชิงคอมพิวเตอร์**

(ภาษาอังกฤษ): **The studies of Morphogenesis by using statistical physics, Mathematical Modeling and Computer Simulations**

คณะผู้วิจัย

ชื่อหัวหน้าโครงการ **ผศ. ดร. วรรณพงษ์ เตรียมโพธิ์**
ภาควิชาฟิสิกส์ คณะวิทยาศาสตร์ มหาวิทยาลัยมหิดล

ชื่อนักวิจัยที่ปรึกษา **ศ. ดร. อิ มิง ถัง**
ภาควิชาฟิสิกส์ คณะวิทยาศาสตร์ มหาวิทยาลัยมหิดล

สนับสนุนโดยสำนักงานกองทุนสนับสนุนการวิจัย

(ความเห็นในรายงานนี้เป็นของผู้วิจัย สกว. ไม่จำเป็นต้องเห็นด้วยเสมอไป)

Content

บทคัดย่อ

ลักษณะและสมบัติเกี่ยวกับมอร์ฟอร์จีนีสิสของระบบของสิ่งมีชีวิตได้ถูกศึกษาในแง่มุมต่างๆโดยอาศัยวิธี ฟิสิกส์เชิงสถิติ การสร้าง แบบจำลอง คณิตศาสตร์ และการทดลองเชิงคอมพิวเตอร์ โดยการผสมผสานวิธีดังกล่าวข้างต้นหรือการบูรณาการวิธีวิจัยอย่างเหมาะสม ทำให้เราสามารถเข้าใจถึงระบบการเจริญของเนื้องอก และแบททีเรีย leptospira ในบางแง่มุม นอกจากนี้ผลจากความพยายามในการสร้างแบบจำลองเพื่อใช้ศึกษาเรื่องนี้ ได้นำไปสู่แบบจำลองที่ใช้ในการอธิบายปรากฏการณ์เกี่ยวกับระบบทางกายภาพ ถึงแม้ว่าโครงการวิจัยจะถูกปิดด้วยผลงานที่ได้รับการตีพิมพ์อย่างน้อย 4 ชิ้น งานวิจัยในลักษณะต่อยอดจากที่ได้เริ่มจะยังคงดำเนินต่อไป

Abstract

Various features and characteristics concerning morphogenesis were studied by using statistical physics, mathematical modeling and computer simulations. With the optimal combination of the integrated approaches, it results the success of understanding the growth of the tumor and bacteria in some aspects. The by product of these studies are the understanding of some physical systems. Even this project is closed and were able to deliver 4 papers the follow-up studies will be continued.

Executive Summary

In this section we shall give some brief details of our work. The more lengthy details are deferred to the attached manuscripts.

1.1. Subproject 1: Analytic approach of the non-equilibrium biological systems

(The work in this part has been in collaboration with Professor I-Ming Tang and Mr. Jirasak Wongekabutr, from dept. of physics , Mahidol university)

The activities in this subproject have been progressing well. Even we have not yet applied the stochastic PDE including noise term as proposed, we instead were able to use the exact lattice calculation in combination with the non-equilibrium master equation to study the simple system of the particles (could also be living cells) exposed to the external field. We shall do experiment relating to this model later (some details in the subproject 4). We have chosen to study small systems as a first step model consisting of two and four particles having two or three possible values of some parameters. Applying periodic boundary conditions, hard core or exclusion volume constraint and imposing conservation of particle numbers via Kawasaki type dynamics (particle-hole exchange). We can set up the stochastic master equations for the case of two particles, one positive and one negative particle in 2x3 lattice system is as follows (the details are deferred to paper):

$$
\begin{aligned}
\partial_t P_1 &= -(2+2x)P_1 + 2P_2 + 2xP_3 \\
\partial_t P_2 &= 2xP_1 - (4+2x)P_2 + 2P_3 + 2P_5 \\
\partial_t P_3 &= 2P_1 + 2xP_2 - (4+2x)P_3 + 2P_4 \\
\partial_t P_4 &= 2P_3 - 4P_4 + 2xP_5 \\
\partial_t P_5 &= 2P_2 + 2P_4 - (2+2x)P_5
\end{aligned}
\qquad (1)
$$

where $x = e^{-E}$, E is the external field, and P_i is the probability distribution associated with each particle configuration.

With the equation above, we were able to calculate the exact solutions of the steady state relative probability density function associated with each configuration of the small systems. The theoretical studies of this simple model is finished and the paper on the results is also accepted for publication in the *journal of the Korean Physical Society*

As the results of very fruitful conlaboration working on this research area, we continue our work by generalizing our model by applying the technique of Monte Carlo simulation to investigate the influence of the temperature on the disordering dynamics of the binary alloys system. We believe that the dynamics used in this work can be applied to study the mechanism of some biological system. We have finished some works on this subproject and were able to publish one international paper as attached on the back of this report.

OUTPUT: 2 accepted international paper.

1.2. Subproject 2: Computer simulations of cell colony growth

(The work in this part has been in collaboration with Ms. Ankana Kitichatt, from dept. of mathematics , Mahidol university)

As proposed, we have investigated the cellular automaton model describing immune system surveillance against cancer under and without the influence of magnetic field. In this model, we consider the system of cancer growth that consists of

(i) cancerous(abnormal) cells [C]

(ii) dead cancer cells [D]

(iii) effector (cytotoxic) cells [E_0]

(iv) complexes produced by the cytotoxic process [E]

We took into account processes of cell-mediated immune response to cancer simplified as follows;

P1: the proliferation of cancerous cells with (rate k_1).

$$C \xrightarrow{k_1'} 2C$$

P2: the Cytotoxic process with (rate k2) and the dissociation of complexes (rate k3)

$$C + E_0 \xrightarrow{k_2} E \xrightarrow{k_3} E_0 + D$$

P3: the dissociation of dead cells with (rate k_4)

$$D \xrightarrow{k_4}$$

We have a constraint that

$$E + E_0 = constant$$

We then translate these information into Cellular Automaton computer simulation rules. We measured the time evolution of number of cancer cells, the total cells and other relevant parameters. Also we plan to study the pattern formation or morphology of cell colonies. Below, we show the preliminary results of the computer simulation.

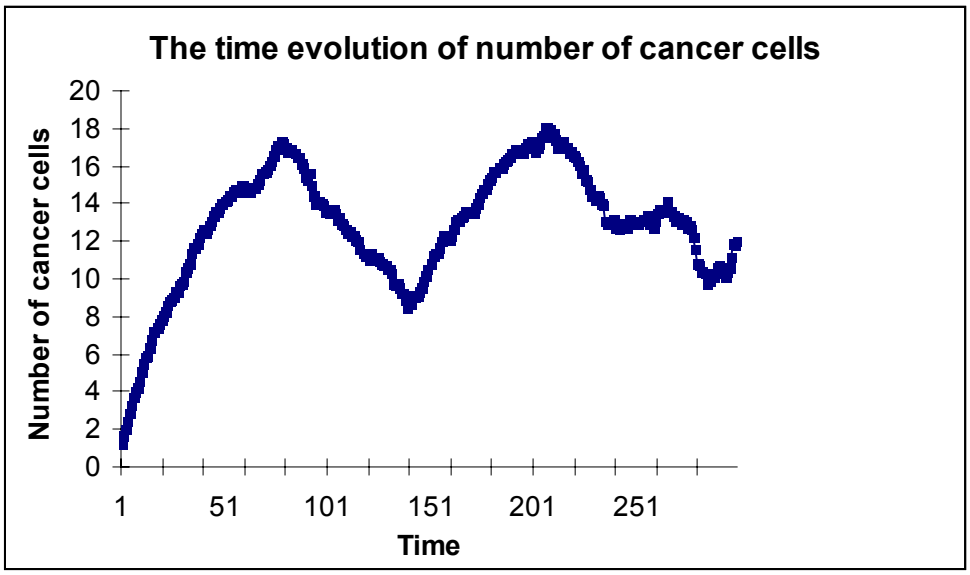

Figure 1. Shows the time evolution of the number of cancer cells.

Model of cancerous growth with magnetic field

We will apply a very similar algorithm as in previous one except here we include the cell movement and some internal degrees of freedom of the system under the influence of magnetic field. The computer programming models are on going processes. The mathematical model is also being formulated.

OUTPUT: 1 international submitted paper.

1.3. Subproject 3: Stochastic modeling and fractal analysis of biological and medical systems

(The work in this part has been in collaboration with Assistant Professor Sutatip Bhamarapravati, from dept. of Plant science, Mahidol university)

Stochastic modeling and fractal analysis is widely used in many scientific field, including the study of pattern formation and morphology of the biological system. It is a convenient method to define the complexity of natural structures. The aim of this investigation was to apply the stochastic modeling and fractal geometry as tools to characterize the growth pattern or morphology. Our works included both theoretical modeling of the relevant model and the experiment of antifungal activity against *Colletotrichum gloeosporioides* using the magnetic field. .

OUTPUT: 1 international accepted paper.

1.4. Subproject 4: Experiments of magnetic effects on biological system

(The work in this part has been in collaboration with Associate Professor Galayanee Doungchawee, from dept. of Pathobiology, Mahidol university)

We have been investigating the influence of a magnetic field on the growth rate, growth pattern formation and other relevant parameters of *Leptospir*a bacteria, under magnetic fields with the magnetic flux densities varying from 0.6 gauss (geomagnetic field) to 2000 gauss. Briefly, *Leptospira* was cultured in the tube at controlled temperature, and light intensity. Permanent magnet with the magnetic flux densities 0.6, 1000, and 2000 gauss were placed beside a culture tube for 24, 48 and 72 hours. We monitor the growth rate, growth pattern

formation and other relevant parameters to characterize the growth of this bacteria due to the magnetic field effect. To do so, we apply the image processing, statistical analysis, fractal analysis, and so on.

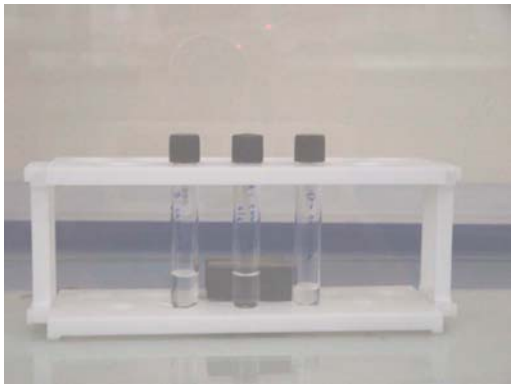

Figure 3. Picture of culture system under static magnetic field.

This is an ongoing process and we expect to learn some interesting things from these studies. Now, we have preliminary results that show effect of magnetic field on the growth behavior of this deadly bacteria. We believe and hope that this study will make a lot of impact in the public health in Thailand.

OUTPUT: 1 accepted international paper.

The details of the research work

The details of each research subproject are shown in the attached documents. They are

1. Random walk on a plane-spin rotator system: Continuum theory and Monte Carlo simulations
2. Explicit Calculations on small Non-equilibrium Driven lattice gas models
3. Vacancy-mediated disordering process in Binary alloys at finite temperatures : Monte Carlo Simulations
4. Effects of static magnetic fields on the growth of leptospire, *Leptospira interogans* serovar *canicola* : Immunological reactivity and cell division
5. Stochastic modeling of the growth of avascular tumor growth(Draft)

Output

Total Projects outputs and Activities

Outputs	No.
1. Papers submitted in international journal	5
2. Paper accepted for publication in international journals	4
3. Papers in conferences.	0

6. Random walk on a plane-spin rotator system: Continuum theory and Monte Carlo simulations

ScienceAsia 2003; 29: 279-289 มี No impact factor

7. Explicit Calculations on small Non-equilibrium Driven lattice gas models

Journal of the Korean Physical Society 2003; 207-214 มี impact factor 1.239

8. Vacancy-mediated disordering process in Binary alloys at finite temperatures : Monte Carlo Simulations

Journal of the Korean Physical Society, In press มี impact factor 1.239

9. Effects of static magnetic fields on the growth of leptospire, *Leptospira interogans* serovar *canicola* : Immunological reactivity and cell division

Journal of Bioscience and Bioengineering, In press, มี impact factor 0.78

10. Stochastic modeling of the growth of avascular tumor growth(Draft)

To be submitted

Supplement information

They include

11. Random walk on a plane-spin rotator system: Continuum theory and Monte Carlo simulations
12. Explicit Calculations on small Non-equilibrium Driven lattice gas models
13. Vacancy-mediated disordering process in Binary alloys at finite temperatures : Monte Carlo Simulations
14. Effects of static magnetic fields on the growth of leptospire, *Leptospira interogans* serovar *canicola* : Immunological reactivity and cell division
15. Stochastic modeling of the growth of avascular tumor growth(Draft)

Random Walk on a Plane-Spin-Rotator System:

Continuum Theory and Monte Carlo Simulations

Wannapong Triampo[a,d*], Darapond Triampo[b], I-Ming Tang[a,d], Yongwimon Lenbury[c]

[a] Department of Physics, Faculty of Science, Mahidol University, Bangkok 10400, Thailand

[b] Department of Chemistry, Faculty of Science, Mahidol University, Bangkok 10400, Thailand

[c] Department of Mathematics, Faculty of Science, Mahidol University, Bangkok 10400, Thailand

[d] Capability Building Unit in Nanoscience and Nanotechnology, Faculty of Science, Mahidol University, Bangkok 10400, Thailand

*Corresponding author, E-mail:wtriampo@yahoo.com

ABSTRACT

We introduce a Plane-Spin-Rotator model (PSR model) as one of a myriad of non-equilibrium statistical mechanics models governed by stochastic dynamics. The system consists of a one-dimensional chain of lattice sites in which each site is attached with a spin initially in the ordered state e.g., pointing in the same direction. We incorporate the effects of a non-equilibrium phenomenon by giving the system a dynamics. Namely we put a random walker (RW) or a Brownian agent at the origin or in the middle of the lattice chain at

the beginning and let it execute pure unbiased random walk to disorder i.e., to destroy the line up of the spins. The local update rule whereby the system changes periodically from one state to another is that each time step as the random walker moves it has a certain probability to rotate the spin or change the angle $\Theta(x,t)$ between the x-axis and the spin. We find the nontrivial statistics of $\Theta(x,t)$ due to this and other simple stochastic (Markovian type) model such as $\langle \cos\Theta(0,t)\rangle$ and $\langle \sin\Theta(0,t)\rangle$ do not behave in sinusoidal fashion as one might expect. These functions and other can be calculated analytically exploiting the results from its "cousin" model introduced in *Physical Review E, Vol. 59, no. 5 p.5127*. Excellent agreement from theoretical and Monte Carlo computer simulation results is found.

KEYWORDS: Stochastic process, Random walk, Brownian, spin, Monte Carlo, non-equilibrium statistical mechanics

1 Introduction

Random walk (RW) or Brownian motion (continuous limit counter part) is one of the fundamental processes in nature. Originally observed in the jiggly irregular motion of pollen grains suspended in water by the English botanist Robert Brown. It was first cast into the mathematical

language by Einstein in 1905[1]. The random walk is one of the most studied problem and versatile concepts in statistical physics. Reif[2] uses the RW to introduce many of the basic and essential concepts of statistical mechanics, while Feller[3] utilizes the same subjects to illustrate the concepts of probability. To physicists and mathematicians, the random walk is a basic paradigm in stochastic processes and is worthy of many monographs. The most recent ones are those by Weiss[4] and Hughes[5]. The theory of random walk has attracted much theoretical attention over the past sixty years due to its numerous application in the physics[6], astronomy[7], chemistry[8], biological science[9], and even social science[10]. The reason for the multiple connections between the RW and the many different questions of current and permanent interest in science is the mathematics. A very rich field of research has built up around the behavior of RW interacting with an environment. A good example being the diffusion of electrons in disordered medium[11]. One can also consider a RW being the disordering agent in its environment[12-13].

Thanks to the detailed studies of the DC[12-13] we found an interesting application and have casted into the new model presented in this paper. We shall call it the Plane-Spin-Rotator model (PSR model). Briefly, this model consists of a RW in one dimension lattice. Each lattice site element is described by the spin lying in a plane like a clock or

rotator, initially all pointing in the same direction. As the RW wanders through, it has a certain probability to rotate the spin or change the angle between the x-axis and the spin direction, $\Theta(x,t)$. The RW is not affected by the environment in any way. Thus if we start with a system in which all spins exist in the same state (e.g. zero $\Theta(x,t)$) or the *ordered* initial configuration and introduce the random walker at origin $x=0$, then after some time, there will be a region around the origin in which the elements will be found in the mixture of various values of $\Theta(x,t)$. An interesting question concerns the degree of disordering which exists for elements within this region namely x-component or $\cos(\Theta(x,t))$ and y-component $\sin(\Theta(x,t))$ (projections of the spin on to the x and y axes). We find that the statistics due to this such simple stochastic model is nontrivial and can be derived analytically by exploiting the results from DC.

The paper is organized as follows. In Section II, we recap our previous work on DC. In Section III, we define our model and discuss which quantities of interest is to be investigated. We then turn to our findings. In Section IV we calculate the predicted analytic results obtained in the first subsection and compare it with the detailed Monte Carlo in the following subsection. Finally, we summarize and present some comments and open questions.

2 Recapitulation

In this section we give a very brief review of the main ideas and some of the results contained in DC which will be of use to the present work. The process of a RW in a binary medium is first modeled on a hypercubic lattice of dimension d . A position of the RW is denoted by a lattice vector $\vec{R}(t)$. In a time step δt the RW has a probability p to move to one of its $2d$ nearest neighbor sites. In making such a jump, there is a probability q that the element on the site will switch to a new value. The elements are described by spin variables $\sigma_{\vec{r}}$ (where $\vec{r}$ denotes a discrete lattice vector) which may take the values ± 1 (see Fig. 1). The spin variables encode the information about the disordering process. For example in the data corruption process we label uncorrupted bits (of value 1) by spin $+1$ and corrupted bits (of value 0) by -1 . [We will often be using the terms "magnetization density" and "global magnetization" which may be simply translated as "density of disorder" and "total amount of disorder".]

We can define the dynamics via the probability distribution $\mathrm{P}(\vec{R}, \{\sigma_{\vec{r}}\}, t)$ which is the probability that at time t , the RW is at position $\vec{R}(t)$ and the spins have values given by the set $\{\sigma_{\vec{r}}\}$. This distribution evolves according to a master equation[14] which takes the form

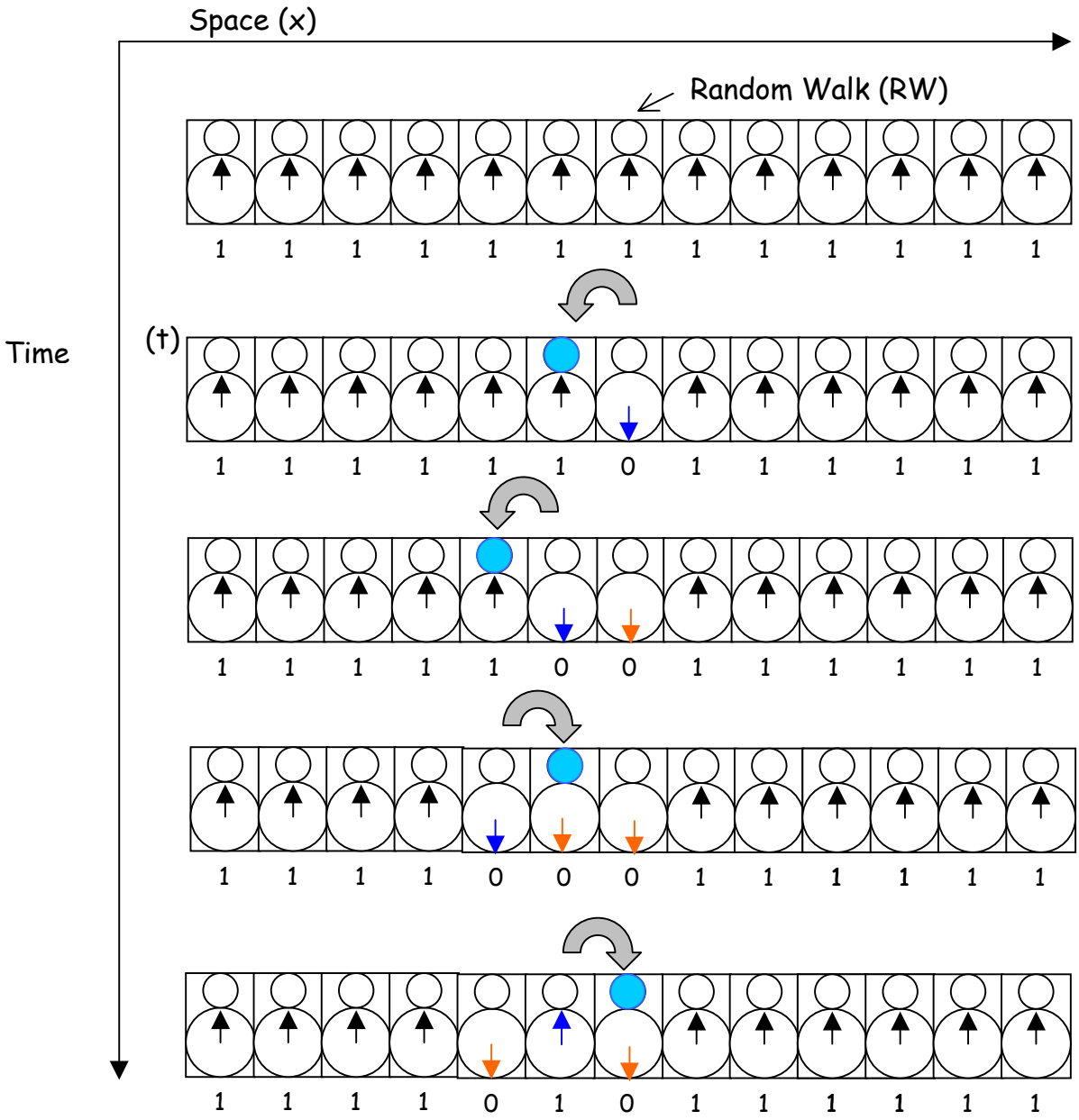

Figure 1. Illustration of the data corruption processes for $d = 1$ *and* $q = 1$*. The initial uncorrupted state is shown on the top, with the RW represented by the filled circle. From the top, we show a typical walk of 4 steps. The RW switches a bit each visit, so those bits visited an even number of times are restored to their original value.*

$$P(\vec{R},\{\sigma_{\vec{r}}\},t+\delta t) = (1-p)P(\vec{R},\{\sigma_{\vec{r}}\},t) + \frac{p(1-q)}{2d}\sum_{\vec{l}} P(\vec{R}+\vec{l},\{\sigma_{\vec{r}}\},t)$$

$$+ \frac{pq}{2d}\sum_{\vec{l}} P(\vec{R}+\vec{l},...,-\sigma_{\vec{R}+\vec{l}},...,t) \qquad (1)$$

where $\{\vec{l}\}$ represents the $2d$ orthogonal lattice vectors (which have magnitude l).

In DC an alternative continuum description was obtained by viewing the process as a stochastic cellular automaton (SCA)[15]. The process is then defined in terms of the position $\vec{R}(t)$ of the RW, and the coarse-grained density of disorder (or magnetization density) which is defined in a small region of space at a specific time, is a functional of $\vec{R}(t)$. In some sense, one may view this in the same spirit as a Langevin description of a stochastic process described at a more fundamental level by a master equation. Taking the continuum limit of this description yields a simple Langevin equation for the position of the RW

$$\frac{d\vec{R}}{dt} = \vec{\xi}(t) \qquad (2)$$

where $\vec{\xi}(t)$ is a noise term, each component of which is an uncorrelated Gaussian random variable with zero mean (i.e. $\xi_i(t)$ is a white noise process). The correlator of $\vec{\xi}(t)$ is given by

$$\left\langle \xi_i(t)\xi_j(t') \right\rangle = D\delta_{i,j}\delta(t-t') \qquad (3)$$

Here and from now on, angled brackets indicate an average over the noise (or equivalently the paths of the RW). The RW is chosen to reside initially at the origin: The evolution of the magnetization density ϕ is described by

$$\partial_t \phi(\vec{r},t) = -\lambda\phi(\vec{r},t)\Delta_{\bar{I}}(\vec{r}-\vec{R}(t)) \quad (4)$$

This equation may be integrated to give the explicit functional solution

$$\phi(\vec{r},t) = \exp[-\lambda\int_0^t dt'\,\Delta_{\bar{I}}(\vec{r}-\vec{R}(t'))] \quad (5)$$

The above solution is obtained for an initial condition $\phi(\vec{r},0) = 1$ which we shall use exclusively. In terms of the original lattice model, it corresponds to choosing all the spins to have the initial value of +1, so that we measure the subsequent disorder of the system by counting the number of minus spins in the system.

In DC we only use the continuum description to generate results for various average quantities. The simplest quantity to consider is the mean magnetization density fro d=1 given by

$$m(\vec{r},t) = \langle\phi(\vec{r},t)\rangle = \sum_{n=0}^{\infty}(-\lambda)^n \chi_n(x,t) \ , \quad (6)$$

where $\chi_0(x,t) = 1,$ and for $n > 0,$

$$\chi_n(x,t) = \frac{1}{n!}\left\langle\left[\int_0^t d\tau\,\delta(x - R(\tau))\right]^n\right\rangle. \quad (7)$$

In DC, it can be shown that

$$\chi_n(x,t) = \int_0^t d\tau_1 \int_0^{\tau_1} d\tau_2 \ldots \int_0^{\tau_{n-1}} d\tau_n\, g(0,\tau_1-\tau_2)\ldots \times g(0,\tau_{n-1}-\tau_n)\, g(x,\tau_n) \ , \quad (8)$$

where $g(x,t) = (2\pi Dt)^{-1/2} \exp(-x^2/2Dt)$ is the probability density of the random walk. Due to the structure of Eq (8) which is an n-fold convolution, we apply the temporal Laplace transform and have (for n>0)

$$\chi_n(x,s) \equiv \int_0^\infty dt e^{-st} \chi_n(x,t) = \frac{1}{s} g(0,s)^{n-1} g(x,s), \tag{9}$$

where

$$g(x,s) = \frac{1}{(2DS)^{1/2}} \exp\left[-\left(\frac{2S}{D}\right)^{1/2} |x|\right]. \tag{10}$$

where $g(x,s)$ is the Laplace transform of diffusion equation Green function.

Summing over these function as formulated in Eq. (6) we find

$$m(x,s) = \frac{1}{s}\left[1 - \frac{\lambda g(x,s)}{1+\lambda g(0,s)}\right]. \tag{11}$$

This exact result allows one to extract a great deal of statistical information about the process. First, one can simply invert the Laplace transform to find the average magnetization density (or average density of disorder relative to 1/2) as a function of $\vec{r}$ and t Explicit forms are given in DC, for $d = 1$, the form is

$$m(x,t) = erf\left[\frac{|x|}{(2Dt)^{1/2}}\right] + \exp\left(\frac{\lambda|x|}{D} + \frac{\lambda^2 t}{2D}\right) \times erfc\left[\lambda\left(\frac{t}{2D}\right)^{1/2} + \frac{|x|}{(2Dt)^{1/2}}\right] \tag{12}$$

where $erf(z)$ and $erfc(z)$ are error function[15]. Considering the long time behavior of the above expression, we find that the average magnetization density at the origin $(x = 0)$ decays asymptotically as

$$m(0,t) = \left(\frac{2D}{\pi\lambda^2 t}\right)^{\frac{1}{2}}\left[1 + O\left(\frac{D}{\lambda^2 t}\right)\right] \qquad (13)$$

We note here that the continuum solution has the important property that $\left\langle \phi(\vec{r},t;\lambda)^n \right\rangle = \left\langle \phi(\vec{r},t;n\lambda) \right\rangle$. This allows us to utilize the exact solution to reconstruct the probability density for the magnetization density.

3 Model

In this section we shall formulate PSR model using the continuum theory as used in DC. It is quite obvious as we mention in DC that formulation using the discrete theory and continuum theory is equivalent. We also want to stress that this is just the alternative method of characterizing the evolution of the system other than using the evolution of the probability distribution of the configuration via the master equation. We start by defining $\vec{\sigma}(x,t) = (\cos(\Theta(x,t)), \sin(\Theta(x,t))) \equiv (\sigma_1(x,t), \sigma_2(x,t))$ as spin variable. Since we are interested in how the angle $\Theta(x,t)$ changes with time as RW wandering through the lattice system, we use the dynamics similar to that use in DC except now the RW interacts with the lattice by rotating the spin as the result of changing $\Theta(x,t)$ (for $d = 1$, see Fig. 2). The local update rule which causes the system to change periodically from one state to another is that each time step as the RW makes a random jump to one of its $(2d)$ nearest neighbors, the RW has a certain probability (here

$p = 1, q = 1)$ to rotate the spin or change the angle between the x-axis and the spin, $\delta\Theta(x,t)$. We write the local rules for the process in the spirit of a stochastic cellular automata (SCA). The local rules for such process are easily written down and are

$$R(t + \delta t) = R(t) + l(t) \tag{14}$$

$$\Theta(x, t + \delta t) = \Theta(x, t) + \delta_{x, R(t)} \tag{15}$$

We are interested in a continuum limit of these two rules. The first is nothing more than a random walk. We take the lattice position $R(t)$ to be a continuum quantity, and we replace the random unit lattice position l(t) by continuum $\xi(t)$, which is an uncorrelated Gaussian random variable (a white noise process) reflecting the random process that has zero configuration average or average over the noise (or equivalent to the paths of RW).

$$\langle \xi(x,t) \rangle = 0 \tag{16}$$

The correlator or the second moment of the noise is given by

$$\langle \xi(x,t)\xi(x',t') \rangle = D\delta(x - x')\delta(t - t') \tag{17}$$

Relation (11) implies that the noise has no correlations in space and time. Then, on taking $\delta t \to 0$, equation (10) assumes the form

$$\frac{dR}{dt} = \xi(t) \tag{18}$$

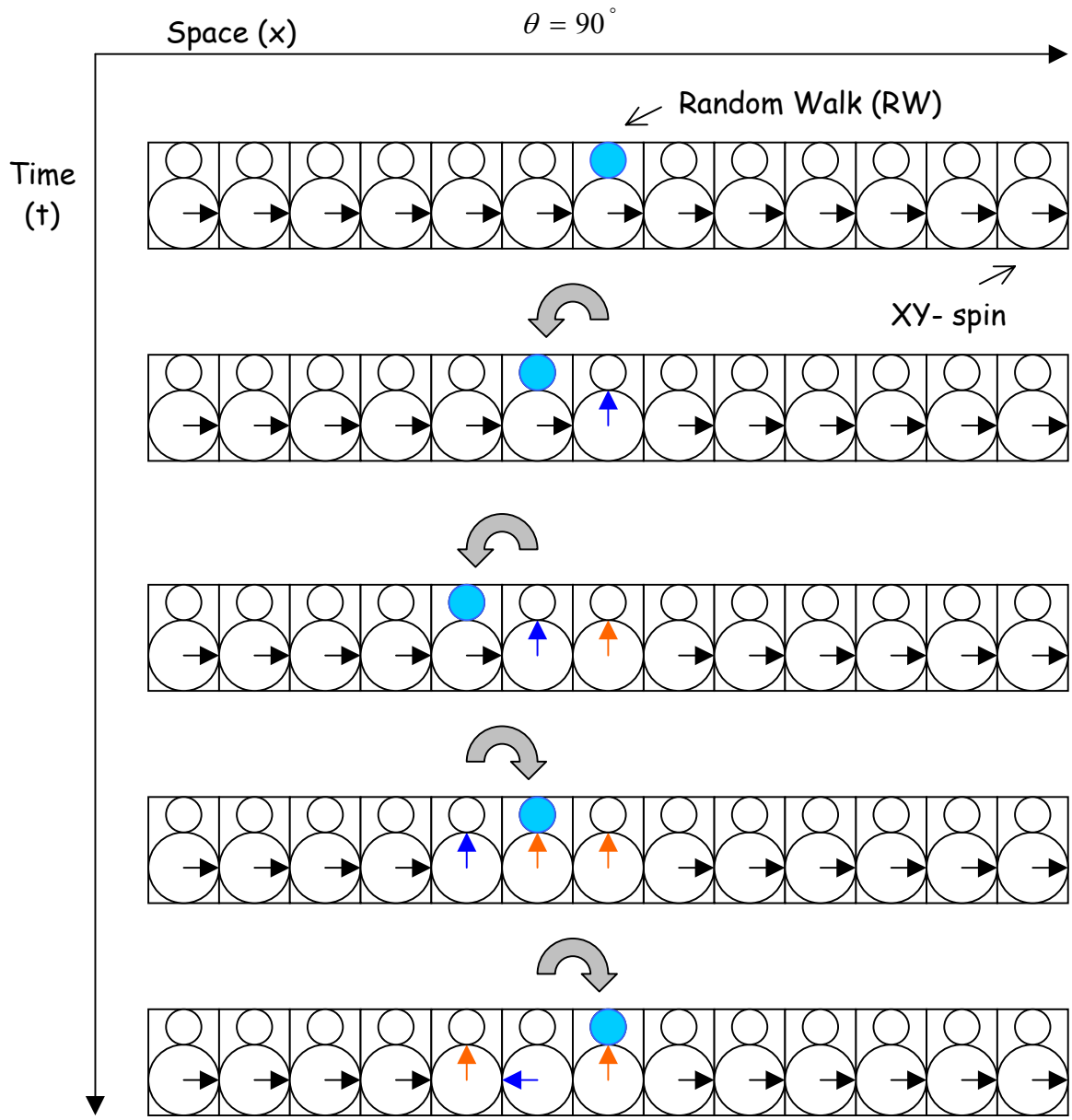

Figure 2. Illustration of the Plane-Spin-Rotator model for $d = 1$. *The initial* $(t = 0)$ *ordered state is shown on the top with the RW represented by the filled circle and the spin is underneath of each RW. On downward order we show a typical (1 from* 2^5*) 5 steps.*

which is the familiar equation for a continuum random walker where D is the diffusion constant[14]. The second SCA rule is more complicated to generalize to continuum. Moving the first term over to the LHS which may then be taken to be time derivative of $\delta t \to 0$. The rest piece resembles a constant term centered at $x = R$

$$\partial_t \Theta(x,t) = \lambda \delta(x - R) \tag{19}$$

where λ is a phenomenological parameter which describes how strongly the spin is coupled to the RW. We stress that the field Θ is a function of the continuous space and time variables x and t, and a functional of the path $R(t)$ of the RW. As we pointed out in DC paper that this continuum equation (15) is not strictly well derived from Eq. (11), as we have not rigorously proved that the continuum limit exists. In fact, we shall find that for $d \geq 2$, the lattice scale is crucial, and consequently we must soften the Dirac δ function to more well defined sharply peaked function.

However, from the following results we will see the good agreement between the data and the analytic results to support our assumption.

Having shown a heuristic derivation of the continuum theory based on a SCA for the case in which the RW always moves, we proceed to the next section in which we present a comprehensive solution in one dimension.

4 Results

In this section we will present some analytic results and some detailed Monte Carlo simulation results.

Analytic results

Here, we are interested in solving Eq. (15) and analyze how the angle $\Theta(x,t)$ evolves with time. Thanks to the nature of the model, one of the positive features of the continuum theory described by the Eq. (15) is that one may immediately integrate the equation to find $\Theta(x,t)$ as an explicit functional of the path of the RW. We first perform a dimensional analysis to be used as a reference in the future reference.

Letting L be the dimension of length and T be the dimension of time, the dimensions of the significant terms are

$$[R] = L$$

$$[\xi] = \frac{L}{T}$$

$$[\xi^2] = \frac{L^2}{T^2} = \frac{[D]}{T} \Rightarrow [D] = \frac{L^2}{T}$$

$$[\partial_t \Theta] = \frac{1}{T} = \frac{[\lambda]}{L} \Rightarrow [\lambda] = \frac{L}{T}$$

$$\left[\frac{\lambda^2 t}{D}\right] = \frac{L^2}{T^2} T \frac{T}{L^2} = 1$$

$$\left[\frac{|x|\lambda}{D}\right] = L.\frac{L}{T}\frac{T}{L^2} = 1$$

$$\left[\frac{|x|}{\lambda t}\right] = \frac{L}{T}\frac{T}{L} = 1$$

Next, we integrate Eq. (15), and get

$$\Theta(x,t) = \lambda \int_0^t dt' \delta(x - R(t')) . \qquad (20)$$

This solution requires the initial condition $\Theta(x,0) = 0$. It is important to note here that $\Theta(x,t)$ is non-negative for all x and t. To get the stochastic properties that we want, we connect these results with those in DC given in section 2. To do this, we set up the solution to Eq. (16) as

$$\Omega(x,t) \equiv \left\langle e^{i\Theta(x,t)} \right\rangle = \left\langle \exp\left[i\lambda \int_0^t dt' \delta(x - R(t')) \right] \right\rangle . \qquad (21)$$

We rewrite Eq. (5) as

$$\left\langle \exp\left[-\tilde{\lambda} \int_0^t dt' \delta(x - R(t')) \right] \right\rangle = erf\left[\frac{|x|}{(2Dt)^{\frac{1}{2}}}\right] + \exp\left[\frac{\tilde{\lambda}|x|}{D} + \frac{\tilde{\lambda}^2 t}{2D}\right] erfc\left[\tilde{\lambda}\left(\frac{t}{2D}\right)^{1/2} + \frac{|x|}{(2Dt)^{1/2}}\right],$$

(22)

where $\tilde{\lambda}$ is just λ (we use the new notation to avoid confusion).

Comparing Eq. (17) with Eq.(18) and keeping in mind that for this case in

$d = 1$ dimension $\Delta\ (\vec{r} - \vec{R})$ can be replaced by delta function $\delta(x - R)$. The parameter $\tilde{\lambda}$ is now $-i\lambda$. The $\Omega(x,t)$ now takes the form

$$\Omega(x,t) = erf\left[\frac{|x|}{(2Dt)^{\frac{1}{2}}}\right] + \exp\left[\frac{-i\lambda|x|}{D} - \frac{\lambda^2 t}{2D}\right] erfc\left[-i\lambda\left(\frac{t}{2D}\right)^{1/2} + \frac{|x|}{(2Dt)^{1/2}}\right]. \quad (23)$$

Recalling the definition of $\Omega(x,t)$, we note that

$$\mathrm{Re}[\Omega(x,t)] = \langle\cos(\Theta(x,t))\rangle \equiv \langle\sigma_1(x,t)\rangle \quad (24\text{-a}),$$

$$\mathrm{Im}[\Omega(x,t)] = \langle\sin(\Theta(x,t))\rangle \equiv \langle\sigma_2(x,t)\rangle \quad (24\text{-b}),$$

where $\mathrm{Re}[\Omega(x,t)]$ and $\mathrm{Im}[\Omega(x,t)]$ are the real and imaginary part of $\Omega(x,t)$ respectively.

Applying the trigonometric theorem, we get

$$\Omega(x,t) = erf\left[\frac{|x|}{(2Dt)^{\frac{1}{2}}}\right] + \exp\left[-\frac{\lambda^2 t}{2D}\right]\left\{\cos\left(\frac{\lambda|x|}{D}\right) - i\sin\left(\frac{\lambda|x|}{D}\right)\right\}\cdot$$

$$\left\{erfc\left(\frac{|x|}{(2Dt)^{1/2}}\right) - \frac{2}{\sqrt{\pi}}e^{-\frac{x^2}{2Dt}}\int_0^{\lambda\left(\frac{t}{2D}\right)^{1/2}} d\beta e^{\beta^2}\sin\left(2\beta\frac{|x|}{(2Dt)^{1/2}}\right) + i\frac{2}{\sqrt{\pi}}e^{-\frac{x^2}{2Dt}}\int_0^{\lambda\left(\frac{t}{2D}\right)^{1/2}} d\beta e^{\beta^2}\cos\left(2\beta\frac{|x|}{(2Dt)^{1/2}}\right)\right\}$$

(25)

It is a straightforward matter after some rearrangement

$$\left\langle \sigma_1(x,t) \right\rangle = erf\left[\frac{|x|}{(2Dt)^{\frac{1}{2}}}\right] + \exp\left[-\frac{\lambda^2 t}{2D}\right] \bullet \{\cos\left(\frac{\lambda|x|}{D}\right) erfc\left(\frac{|x|}{(2Dt)^{1/2}}\right)$$
$$- \cos\left(\frac{\lambda|x|}{D}\right)\frac{2}{\sqrt{\pi}} e^{-\frac{x^2}{2Dt}} \int_0^{\lambda\left(\frac{t}{2D}\right)^{1/2}} d\beta e^{\beta^2} \sin\left(2\beta\frac{|x|}{(2Dt)^{1/2}}\right)$$
$$+ \sin\left(\frac{\lambda|x|}{D}\right)\frac{2}{\sqrt{\pi}} e^{-\frac{x^2}{2Dt}} \int_0^{\lambda\left(\frac{t}{2D}\right)^{1/2}} d\beta e^{\beta^2} \cos\left(2\beta\frac{|x|}{(2Dt)^{1/2}}\right)\} \qquad (26)$$

After more simplification, we get

$$\left\langle \sigma_1(x,t) \right\rangle = e^{-\frac{\lambda^2 t}{2D}} \cos\left(\frac{\lambda|x|}{D}\right) + erf\left(\frac{|x|}{(2Dt)^{1/2}}\right) \cdot \left[1 - e^{-\frac{\lambda^2 t}{2D}} \cos\left(\frac{\lambda|x|}{D}\right)\right]$$
$$+ \frac{2}{\sqrt{\pi}} \exp\left(-\frac{\lambda^2 t}{2D} - \frac{x^2}{2Dt}\right) \cdot \int_0^{\lambda\left(\frac{t}{2D}\right)^{1/2}} d\beta e^{\beta^2} \sin\left(\frac{\lambda|x|}{D} - \frac{2\beta|x|}{(2Dt)^{1/2}}\right)$$

, (27-a)

and

$$\left\langle \sigma_2(x,t) \right\rangle = -erfc\left(\frac{|x|}{(2Dt)^{1/2}}\right) e^{-\frac{\lambda^2 t}{2D}} \sin\left(\frac{\lambda|x|}{D}\right)$$
$$+ \frac{2}{\sqrt{\pi}} \exp\left(-\frac{\lambda^2 t}{2D} - \frac{x^2}{2Dt}\right) \cdot \int_0^{\lambda\left(\frac{t}{2D}\right)^{1/2}} d\beta e^{\beta^2} \cos\left(\frac{\lambda|x|}{D} - \frac{2\beta|x|}{(2Dt)^{1/2}}\right)$$

. (27-b)

Considering the specific value of the above expression, we have, for $x = 0,$

$$\left\langle \sigma_1(0,t) \right\rangle = e^{-\frac{\lambda^2 t}{2D}}, \qquad (28\text{-a})$$

and

$$\left\langle \sigma_2(0,t) \right\rangle = \frac{2}{\sqrt{\pi}} \cdot e^{-\frac{\lambda^2 t}{2D}} \cdot \int_0^{\lambda\left(\frac{t}{2D}\right)^{1/2}} d\beta e^{\beta^2} \qquad (28\text{-b})$$

Since we wish to compare our analytic results with the Monte Carlo computer simulation results, we consider the two limits;

$$\left\langle \sigma_2(0,t)\right\rangle = \begin{cases} \frac{2}{\sqrt{\pi}}\cdot\left(\frac{\lambda^2 t}{2D}\right)^{1/2}\cdot\left[1-\frac{2}{3}\frac{\lambda^2 t}{2D}+O\left(\left(\frac{\lambda^2 t}{2D}\right)^2\right)\right]; & \frac{\lambda^2 t}{2D}<<1 \\ \frac{1}{\sqrt{\pi}}\cdot\left(\frac{2D}{\lambda^2 t}\right)^{1/2}\left[1+\frac{1}{4}\frac{2D}{\lambda^2 t}+O\left(\left(\frac{2D}{\lambda^2 t}\right)^2\right)\right]; & \frac{\lambda^2 t}{2D}>>1 \end{cases} \tag{29}$$

From Eq. (25), it can be show that $\left\langle \sigma_2(0,t)\right\rangle$ behaves differently for small and large time with a cross over which can be calculated as follows;

let, $\frac{\lambda^2 t}{2D}=a^2$ we rewrite

$$\left\langle \sigma_2(0,t)\right\rangle = \frac{2}{\sqrt{\pi}}\cdot e^{-a^2}\cdot\int_0^a d\beta\, e^{\beta^2}\ , \tag{30}$$

The value of maximum of the function can be obtained by differentiating with respect to a, and set it to zero, i.e.,

$$\partial_a\left\langle \sigma_2(0,t)\right\rangle\Big|_{a^*} = 0 = 1-2a^* e^{-a^{*2}}\int_0^{a^*} d\beta\, e^{\beta^2} \tag{31}$$

We get

$\left\langle \sigma_2(0,t)\right\rangle_{\max} = \frac{1}{a^*\sqrt{\pi}}$ which is independent of λ and D

Using some trigonometric function identity, we can show that

$$\left\langle \sigma_1^2(x,t)\right\rangle = \left\langle \cos^2\Theta(x,t)\right\rangle = \frac{1}{2}\left\{1+\left\langle \cos\left(2\Theta(x,t)\right)\right\rangle\right\} = \frac{1}{2}+\frac{1}{2}\left\langle \sigma_1(x,t;2\lambda)\right\rangle, \tag{32-a}$$

$$\left\langle \sigma_2^2(0,t)\right\rangle = \frac{1}{2}\left(1-e^{-\frac{2\lambda^2 t}{D}}\right). \tag{32-b}$$

Again we focus on the value of the function at the origin, we have

$$\left\langle \sigma_1^2(0,t)\right\rangle = \frac{1}{2}\left(1+e^{-\frac{2\lambda^2 t}{D}}\right) \tag{33-a}$$

$$\left\langle \sigma_2^2(0,t)\right\rangle = \frac{1}{2}\left(1-e^{-\frac{2\lambda^2 t}{D}}\right) \tag{33-b}$$

We now turn to simulation results.

Monte Carlo simulation results

Our aim in this section is to show the validity of our theoretical results from the previous section. To do so, we have performed Monte Carlo simulations of the discrete version model, defined in section 2. In all of the simulations for which we present results, we have set the hopping rate p of the RW to unity. All of our results are obtained for a one-dimensional chain of sites. The chain length is unimportant, so long as one ensures that the RW never touches the edges in any of its realizations up to the latest time at which data is extracted. We perform an average over 10^6 realizations (or runs). Such simulations require a few days on a DEC Alpha 233 MHz

workstation. In a given run, the RW is moved left or right with equal probability at each time step and the spin it left behind is rotated. Each run starts with the same initial configuration; namely all spins are pointed to the x-direction making zero degree with x-axis.

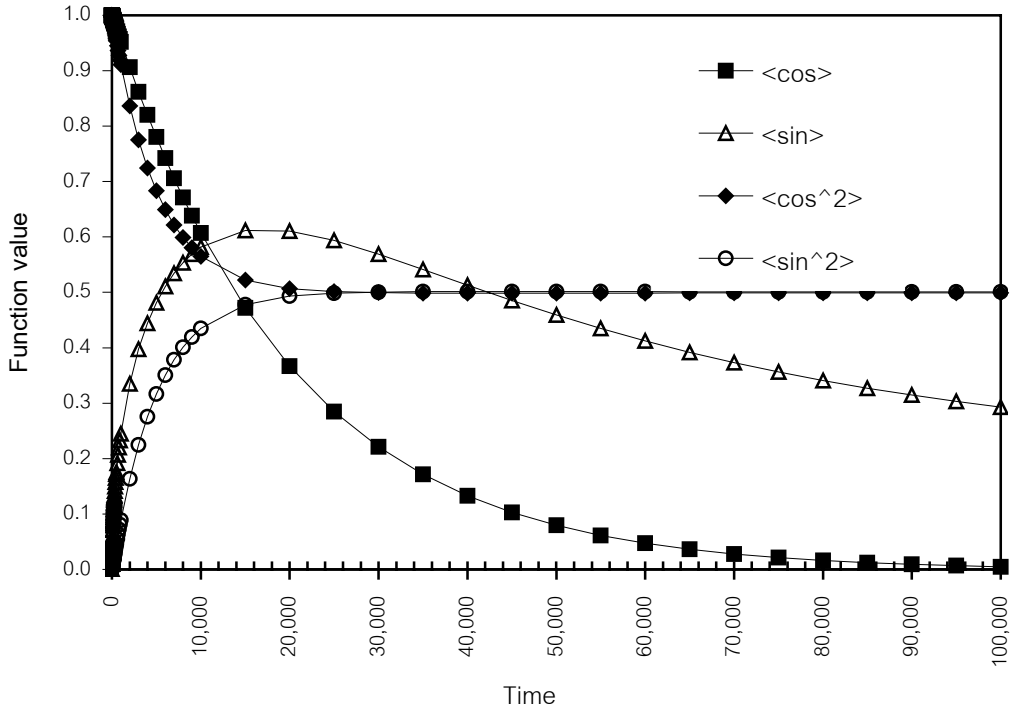

Figure. 3. Plot of simulation data for the $\langle \cos \Theta(0,t) \rangle$, $\langle \sin \Theta(0,t) \rangle$, $\langle \cos^2 \Theta(0,t) \rangle$, *and* $\langle \sin^2 \Theta(0,t) \rangle$.

In Fig. 3 we show the numerical results of all the means of trigonometric function of $\Theta(x,t)$ at origin namely $\langle \cos \Theta(0,t) \rangle$, $\langle \sin \Theta(0,t) \rangle$, $\langle \cos^2 \Theta(0,t) \rangle$, and $\langle \sin^2 \Theta(0,t) \rangle$ versus time. They all appear to have the correct features as theoretically predicted. This confirms the relations given in Eq. (28), Eq. (29), and Eq. (33).

In Fig. 4, we show the semi-log plot of $\langle \cos \Theta(0,t) \rangle$ vs. time. Due to the exponentially function feature as analytically predicted it results in the straight line. Using Excel program to do multiple regression, it shows the good fit with the fitting function $1.005\ e^{-5\times10^{-5}t}$ (r^2 = 0.9996). This emphasize the agreement between the numerical data and Eq. (28)

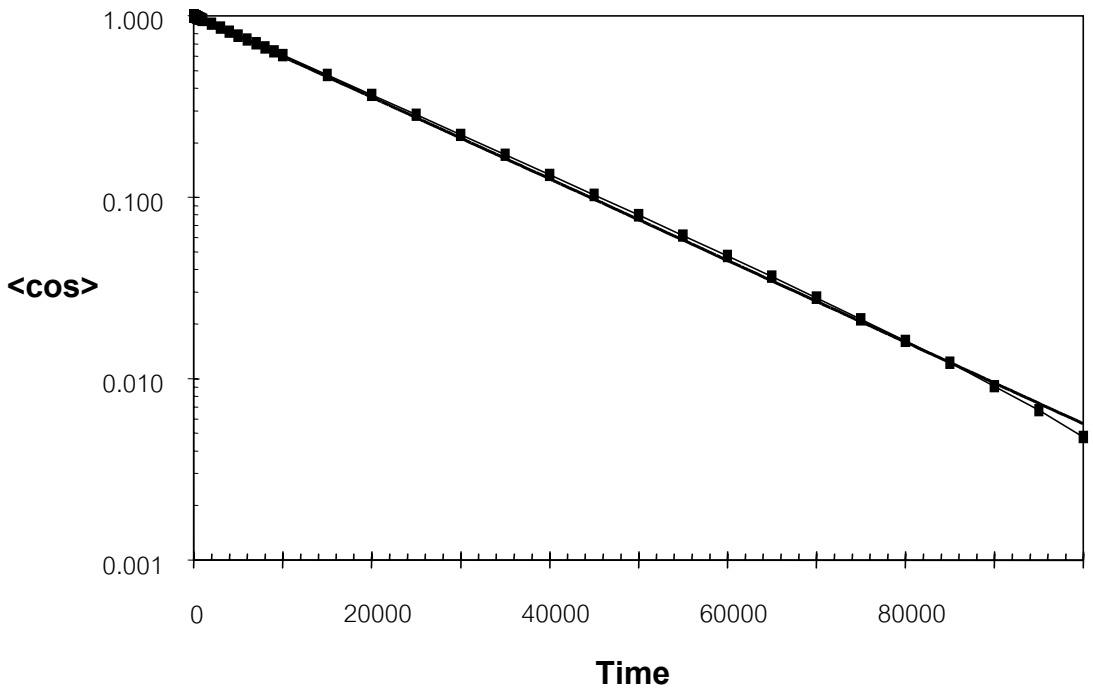

Figure. 4. Semilog plot of $\langle \cos \Theta(0,t) \rangle$ *vs. time. The denser solid line (which is partially obscured by the data) is the regression line with function* $1.005\ e^{-5\times10^{-5}t}$ and $r^2 = 0.9996$

In Fig. 5, to verify the Eq. (29), we log-log plot of the $\langle \sin \Theta(0,t) \rangle$ function versus time. The plot does show two regimes with different power laws as predicted. In the early regime the graph gives the straight line with slope about 0.5 and the fitted function $0.0082\ t^{0.4922}$, with r^2 = 0.9982 which is in good agreement with predicted theory. With the cross-over time about the time step 10,000 to 30,000, it turns into

another scaling law with another slope (predicted slope = -0.5) as seen in later regime. Due to the problem about the computing resources we now have, we consequently did not perform simulation for long time enough to get the convincing data (at least one and haft decade of power law or straight line). Therefore from the data they only confirm the two power law behaviors but not confirm the power law of the later regime. Arguably, we did try to extrapolate the curve to see roughly presumably if its slope were -0.5. We found that the slope could be -0.5. However, in the near future we hope to get more powerful computers to run for longer time with a lot of runs to get the nice curve with the least noise.

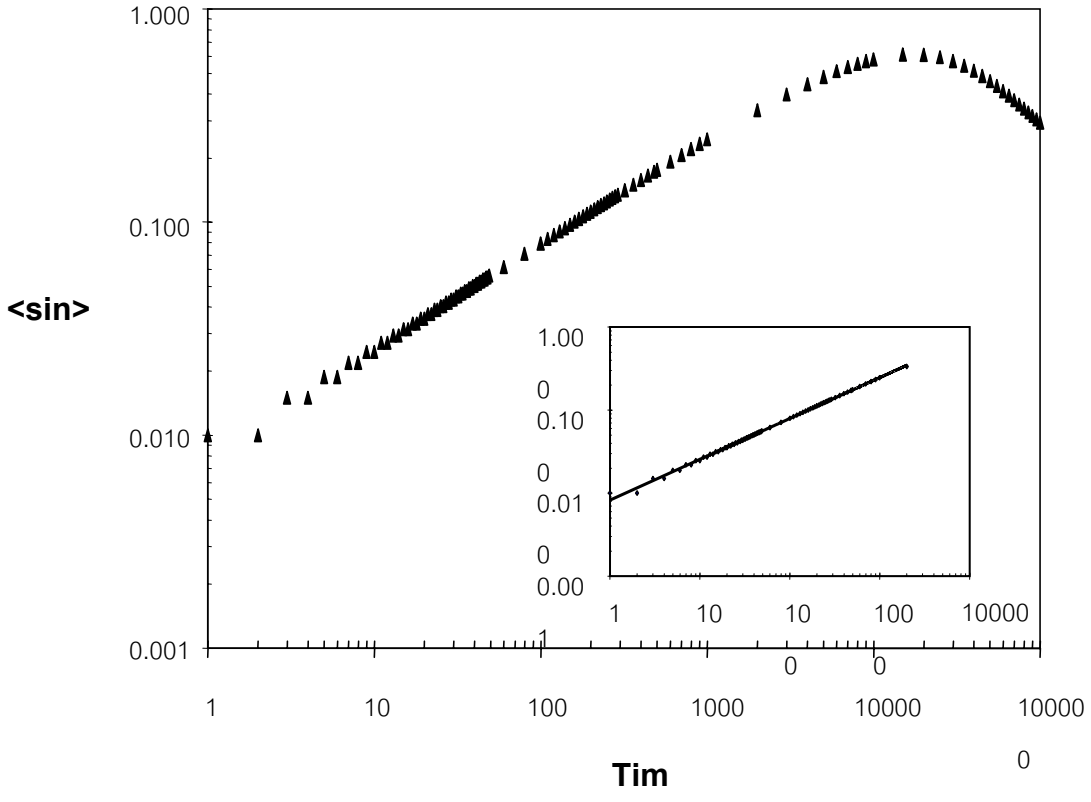

Figure. 5. Log-log plot of $\langle \sin \Theta(0,t) \rangle$ *vs. time to verify the power law behavior of the data. The inset shows the regression line of curve fitting with function* $0.0082\, t^{0.4922}$ and $r^2 = 0.9982$

It should also be mentioned about the lines $\left\langle \cos^2 \Theta(0,t) \right\rangle$ and $\left\langle \sin^2 \Theta(0,t) \right\rangle$. Early, they are controlled by the exponential feature and asymptotically approach to 0.5 afterward as predicted by continuum theory. We end this section by mentioning that all these agreement between the numerical data and the continuum theoretical results provides very strong evidence for validity for the validity of our whole continuum approach.

5 Summary and Conclusion

We have introduced and analyzed a Plane-Spin-Rotator model (PSR model) undergoing disordering, focusing on its stochastic dynamics due to a random walker or Brownian agent. In section 2, we present a review of our previous work on DC and described what motivated us to study this model. In section 3, we formulate the continuum equations of our model by starting from the discrete version on the spirit of stochastic cellular automata, which consists of a RW rotating clocks (or spins) on a lattice as it wanders. The model is non-trivial since the value of Θ depends sensitively on the path of the RW *i.e.* how often the RW has visited the spins. The continuum equation formulation of PSR model has similar feature as in the system which we use before to describe the data corruption model in DC. In section 4, we examine the properties of the continuum theory for $d = 1$. In the first subsection, we derived an exact expression for the evolution of the x and y component of the spin i.e.,

$\cos(\Theta(x,t))$ and $\sin(\Theta(x,t))$. Using a fortuitous property of the original continuum theory in DC, we find that at the origin the average of time variation of x -component for small and large time have the following behavior. For the x -component, it decreases exponentially to zero with the characteristic time scale $2D/\lambda^2$. In contrast, the y -component is proportional to $\sqrt{t}$ for small times and goes like $1/\sqrt{t}$ for large time with the maximum independent of the diffusive and the coupling constant. We have calculated the next moment of both quantities namely $\left\langle \cos^2 \Theta(0,t) \right\rangle$ and $\left\langle \sin^2 \Theta(0,t) \right\rangle$. In the second subsection, we presented our computer experimental results from Monte Carlo simulations of the discrete lattice model. We have measured the temporal variation of all corresponding analytic results predicted. In all cases we find good agreement between our data and the theoretical predictions arising from the continuum model.

In conclusion, we have introduced and solved a model in which a random walker interacts with a spin environment. The benefit from this work is of course the insight into one specific example of the stochastic process mediated by random or Brownian agent. One can view this problem as the disordering process starting from the initially ordered configuration and the degree of disordering increase as time goes on due to the dynamics or local update rule one applied. In DC our primary application is to an environment composed of bits of (two states) data, which the random walker steadily corrupts. We can apply our results to system characterized by more than two states. It remains to be seen

whether one can find a solid application of the models. In the future work, we will explore cases of two or more dimensions of agents or walker. There are many future direction of future work, foremost among which are (i) calculating all quantities in two dimensional space (ii) investigating two point an autocorrelation functions in both one and two dimensions (iii) studying many agents and more generalized coupling to make a stronger connection to real processes.

Acknowledgement

We thank N. Nuttawut, A. Kitichattraporn and S. Sa-nguansin for helpful reading a manuscript and some comments. We also greatly appreciate both referees for their very helpful comments. This research is supported in part by Thai Research Fund through the grant number TRG4580090 and RTA4580005 and MTEC Young Research Group funding MT-NS-45-POL-14-06-G.

References

1. Einstein A (1956) *Investigations on the Theory of the Brownian Motion*. Dover, USA.
2. Reif F (1965) *Fundamentals of Statistical and Thermal Physics*. McGraw-Hill, New York.
3. Feller W (1968) *An Introduction to Probability Theory and Its Applications*, 3rd ed. Wiley, New York.
4. Weiss GH (1994) *Aspects and Applications of the Random Walk*. North Holland, Amsterdam.
5. Hughes BD (1995) *Random Walks and Random Environments*. Clarendon Press, Oxford.
6. Chandrasekhar S (1943) Stochastic problems in physics and astronomy. *Rev Mod Phys* **15**, 1.
7. Weiss GH and Rubin RJ (1983) Random walk: theory and selected applications. *Adv Chem Phys* **52**, 363.
8. Berg HC (1993) *Random Walks in Biology*, expanded edition. Princeton University Press.
9. McGrady GA, Marrow C, Myers G, Daniels M, Vera M, Mueller C, Liebow E and Klovdahl A, et al (1995) A note on implementation of a random-walk design to study adolescent social networks. *Social Networks* **17** (3-4), 251-255.
10. Havlin S and Ben-Avraham D (1987) Diffusion in disordered media. *Adv Phys* **36**, 695.
11. Newman TJ and Triampo W (1999) Binary data corruption due to a Brownian agent. *Phys Rev E* **59** (5), 5172.

12. Triampo W and Newman TJ (1999) Binary data corruption due to a Brownian agent. *Phys Rev E* **60** (2), 1450.

13 Gardiner CW (1985) *Handbook of Stochastic Processes*, 2nd ed. Springer-Verlag, Berlin.

14. Abramowitz M and Stegun IA (1972) *Handbook of Mathematical Functions*, 10th ed. Dover, NY.

15. Wolfram S (1987) *Theory and Applications of Cellular Automata*. World Scientific, Singapore.

Vacancy-mediated disordering processes in binary systems at finite temperature: Monte Carlo simulations

J. Wong-ekkabut, W. Triampo[a,d*], D. Baowan[c] ,D. Triampo[b], I-Ming Tang[a,d], and Y. Lenbury[c]

[a] Department of Physics, Faculty of Science, Mahidol University, Bangkok 10400, Thailand

[b] Department of Chemistry, Faculty of Science, Mahidol University, Bangkok 10400, Thailand

[c] Department of Mathematics, Faculty of Science, Mahidol University, Bangkok 10400, Thailand

[d] Capability Building Unit in Nanoscience and Nanotechnology, Faculty of Science, Mahidol University, Bangkok 10400, Thailand

*Corresponding author, E-mail:wtriampo@yahoo.com

Abstract

We investigated the time evolution of vacancy-mediated disordering process of binary alloys at finite temperature. Qualitatively, we monitor the change of configuration by taking the snapshots sequence , and quantitatively we measure the time dependent disorder and time dependent structure factors for the modulate low temperature. Unlike , the case of when the vacancy execute random walk and bias walk here the vacancy

act as highly active walk experience nonlinear feedback . In comparison with those to previous cases the slope 0.5 of disorder parameter breaks down to become the temperature dependent. For the structure factors, we still get the dip as in infinite temperature case, however, the overall feature change when the temperature becomes finite. The portion of the graph giving the scaling exponent of slope = 1 in the intermediate regime is gradually taken over by the slope = 0.5. This is clearly seen when the wave vectors are small but somewhat obscured when wave vectors are large.

1. Introduction

Motivated by the important role of such processes for real systems especially in the materials science and physics communities such as interface corrosion or erosion phenomena[1-3], and device fabrication[4-5], we shall study a specific model for interactions between an agent and its environment, namely how the system disorders when its kinetics is mediated by an active agent controlled by energetic “feedback” from the environment.

We investigate the kinetic disordering of an initially phase-segregated interacting binary alloy due to a highly mobile vacancy following a rapid increase in temperature. Starting at zero-temperature ferromagnetic ordered configuration with sharp interfaces, we study the temporal evolution of how particles of one species are transported into regions dominated by the other species resulting in the interface roughening or complete destructing depending on the final temperature[see figure 1-4]. Clearly, if the final temperature is sufficiently high, the interface will eventually disappear, resulting in a homogeneous final(mixing) state. While if the temperature are low the “degree of homogeneity” associated with the final configuration would change. In the model, we consider a symmetric binary alloy of A and B atoms which is diluted by a very small number of vacancies $\approx 10^{-5}$ found in most real systems[6]. The vacancy acts as a “catalyst” exchanging with the neighboring particles according to the usual energetic of the (dilute) Ising model[7]. The particle themselves form a passive backgrounds whose

dynamics are slaved to the vacancy motion. Thus , this system corresponds to a real material in which the characteristic time scale for vacancy diffusion is much faster than the ordinary bulk diffusion time. Once again the complete or partial mixing of two materials at an interface play a key role in many physical processes. We mention just one application with huge technological potential for device fabrication. It concerns nanowire etching by electron beam lithography [4]: If a thin film of platinum is deposited on a silicon wafer, inter-diffusion of Pt and Si produces a mixing layer. If this layer is heated locally by, e.g., exposure to a conventional electron beam, silicides, such as Pt_2Si and PtSi, form. The unexposed platinum can subsequently be etched away, leaving conducting nanoscale structures behind. However, the performance of this device requires precisely engineered layer thicknesses and interfaces, and can be significantly affected by disorder including interdiffusion or interfacial fluctuations.

…….

In analogy with the spirit of phase ordering such as phase separation and domain growth[8-16], we will seek to deal with any universal features in the time evolution of the system. In fact, several questions emerge quite naturally such as: Are there characteristic time scales on which the disordering takes place, and how they depend on the system size, temperature, and other controlling parameters?, How do local density profiles and correlation functions evolve with time?, and How do these features respond to changes in the relative concentrations of vacancies and alloy component? Some of these questions had answers but only for the limit of infinitely high temperature where the vacancy executes random walk motion[17]. In this paper we shall devote to study “upquenches” to finite moderate($T>T_c$) and low($T<T_c$) temperatures. This limit is a non-trivial situation since the hopping rates of the vacancy now depend on the spin configuration in its vicinity: this introduces a highly non-linear feedback effect which was absent for Brownian vacancy. If the final temperature remains above the coexistence line of the Ising model, the steady state is still disordered. But the ordered phase will persist if temperature is below Tc. Mathematically to the best of our knowledge there is no exact solutions of non-equilibrium master equation[18] to this problem, therefore, progress relies mainly on computer simulations.

This article is organized as follows. We clarify the studied model and define appropriate time-dependent disorder parameters and structure factors in section II. In section III, the Monte Carlo(MC) simulation result and discussion would be given. We summarize and conclude with some comments in the last section.

2. Model

Consider the discrete model underlying the Monte Carlo simulations. It is defined on a two-dimensional square lattice of dimensions $L \times L$. Each lattice site is denoted by a pair of integer $\vec{r} = (i, j)$. To model the binary systems consisting of the two species of particles, we allow each site can be occupied by either a black particle("spin up"), a white particle("spin down"), or a vacancy("spin zero"). Multiple occupancy is forbidden. One may view this model as the dilute Ising model. Thus the configurations of the model can be characterized by a set of spin variables $\{\sigma_{\vec{r}}\}$ which can take three values: $\sigma_{\vec{r}} = +1(-1)$ for a black(white)particle and $\sigma_{\vec{r}} = 0$ for a vacancy. The number of black (N^+) and white (N^-) particles are conserved and differ by at most 1: $N^+ \approx N^- \cong \frac{1}{2}(L^2)$. To model the minute concentration of vacancies in real systems, we focus on the case where the number of vacancies, $M << N^+, N^-$. In fact, all simulations will be restricted to $M = 1$. The boundary conditions are fully periodic in all directions. The initial configuration is perfectly unstable phase segregated: Black and white particles each fill one half of the system, with a sharp flat interface between them, chosen to lie horizontally along the x axis. The vacancy is located at the interface.

Now we turn to a microscopic dynamics or local update rule. Besides the correlation via the excluded volume constraint, particles and vacancy interact with one another according to a dilute Ising model:

$$\mathrm{H}\left[\{\sigma_{\vec{r}}\}\right] = -J\sum_{\langle r,r'\rangle}\sigma_r\sigma_{r'} \qquad (1)$$

with ferromagnetic , nearest-neighbor coupling $J > 0$. Since the dilution is so small, the behavior of the system is that of the ordinary (non-dilute) two-dimensional Ising model. Thus, it has a phase transition, from a disordered to a phase-segregated phase, at the Onsager critical temperature, $T_c = 2.267...J/k_B$ [19]. The ground state is doubly degenerate consisting of a strip of positive and negative spins, each filling half the system, separated by two planar interfaces. And since the particle-particle interaction are ferromagnetic, a vacancy is accumulated at the interface. This is what we choose to be our initial configuration of the disordering process.

The vacancy performs an active walk or non-linear feed back walk on the lattice with the transition rate, per unit time step (Monte Carlo step) defined as $W\left[\{\sigma_r\}\{\sigma'_r\}\right]$ from configuration $\{\sigma_r\}$ into a new configuration $\{\sigma'_r\}$. Here, only particle-vacancy nearest-neighbor exchanges are allowed. We choose $W\left[\{\sigma_r\}\{\sigma'_r\}\right]$ to be the usual Metropolis rate[20], namely

$$W = \min\{1, \exp(-(1/k_BT)\,\Delta\mathrm{H})\} \qquad (2)$$

where $\Delta\mathrm{H}$ is the energy difference of the system after and before the jump. From this rate, one should expect, as time progresses, the vacancy would disorder the interface when $T > 0$ and completely dissolve it when $T > T_c > 0$.

In the simulations, at each Monte Carlo time step (MCS), one of the four nearest neighbors of the vacancy is chosen at random. The exchange is performed according to the rate defined above and once again no particle-particle exchange is allowed. There are two control parameters for the simulations namely the temperature T and the system size L .The final temperature after up-quench measured in units of the Onsager temperature T_c , varies between $0.5T_c$ and infinity(in the language of Ising model infinite temperature implies energy costs are ignored for system evolution). The system size is 100×100 lattice. Our data are averages over 10^3 realizations (or runs) or more depending on the desired quality of the data.

At time $t = 0$, the system with the phase separation corresponding to $T = 0$ configuration experiences a temperature up-quench to finite temperature. We would like to study the evolution of the system undergoing disordering. We qualitatively monitor the visual temporal evolution and quantitatively measure the following:

(1) Time-dependent disorder parameter

It is the average number of black and white nearest-neighbor pairs, $A(L,T;t)$ as a function of time t. This quantity is related to the Ising energy, as

$$A(L,T;t) \cong L^2 + \frac{1}{2J}\langle H \rangle \tag{3}$$

where $\langle \bullet \rangle$ denotes the time-dependent configurational average over a large number of independent runs.

(2) Time-dependent structure factors.

It is defined as

$$S_{\vec{k}}(t) \equiv \frac{1}{L^2}\left\langle \left| \sum_r \sigma_r(t) \exp(-i\vec{k}\cdot\vec{r} \right|^2 \right\rangle \tag{4}$$

Where $\vec{k} = (k_x, k_y) = \frac{2\pi}{L}(n_x, n_y)$, with n_x and n_y integers. We shall focus on the most interesting structure factors which are those whose wave vector $\vec{k}$ is perpendicular to the initial planar interface. Thus, here we shall focus on $n_x = 0$ and $n_y = 1,2,3,4,5,6...$

3. Results and Discussion

3.1. Visual snapshots

Qualitatively, to obtain a visual impression of the disordering process, Fig. 1, Fig. 2 , Fig 3 and Fig.4 show the evolution of a typical configuration in a 100×100 lattice with $T=\infty,3.5T_c,1.5T_c$,and $0.8T_c$ respectively. In all cases, the initial interface is completely smooth at $t=0$. it begins to slowly break up as time progresses as the vacancy wanders; random walk motion for T=∞ and active walk for finite temperature. The numbers of particles are (inter)diffused into the opposite colored domain and cause the rough interface. As time goes on the degree of homogeneity becomes larger and the interface becomes rougher. Eventually, at steady state, the system corresponding $T>T_c$ become disordered or homogenous mixed state, while those corresponding to $T<T_c$ still phase segregation but with relatively rougher interface. The lower final temperatures, the longer time the system takes to reach the final steady states and approximately is of the order of L^4 (for not very low temperature). Even from the snapshot, one clearly see that in comparison with the infinite temperature case, the final configuration of the finite one shows considerably clear evidence of finite correlation length which once again get larger as the final temperature being set higher. One can see bigger clusters in the compared figures. These are due to the effect of the interaction between particles which become more and more significant as the temperature get cooler. It should be noted that, in all cases the vacancy is equilibrated much faster than the particles, and at the lower temperature, the vacancy reach to steady state later. From this visual impression, it suggested that at least two time scale need to be taken into account namely the time scales that the vacancy and particles reach to equilibrium state.

3.2. Time-dependent disorder parameter

The disordering process is clearly reflected in the disorder parameter $A(L,T;t)$.As shown in figure 6, it increases from $2L-1$ for an initial configuration to the order of L^2

for the equilibrium. Similar to as discussed in [21-22], for not very low temperature one clearly distinguishes three regimes shown schematically in Fig.6 an early regime (E), the intermediate regime (I) and saturation regime(S). It should be noted that the I and S regimes emerge only in a finite system. As the system size increases, the (I) regime spans a widening time range. In [21], they showed that in (I) the systems exhibit dynamic scaling in $A(L,T;t) \approx t^{1/2}$ for infinite temperature. Later in [23] the universality of this scaling relation was extensive studied for the case of high temperature with the external field and they found that the same scaling relation still is valid. For the finite temperature, as extensively studying here was speculated in [22].

One of our goals in this work is to test to what extend the dynamic scaling namely the relation $A(L,T;t) \approx t^{1/2}$ still held when the temperature is especially moderate and low. Here we have extensively performed simulations and curve fitting with nonlinear regression. We found that the slope of the low temperature case are significantly deviated from the slope 0.5.The results show in table [table1].

In table 1,the data analysis was treated by the program Microcal (MT) origin version 6.0. From the intermediated regime, we evaluated the slope with a linear regression which is collected 35 points in the interval more or less 10^5 to 6×10^6 Monte Carlo Steps (MCS) (~1.5 decades). From the table , we can see that at T = 0.5 T_c the slope is 0.0646 with correlation coefficient = 0.99533 and SD = 0.0093 which evidently deviated from 0.5 about 87.08% and at T = 3.5 T_c the slope is 0.48574 with correlation coefficient = 0.99999 and SD = 0.00208 which deviated from 0.5 about 2.85%. Moreover, if the temperature are increased, $T >> T_c$ (infinity temperature), the slope of them increase to 0.5. Therefore ,from all of the results, the rapid change of slopes depend on temperature. We confirm this argument by doing data curve fitting using to fit function as follows. The first one , we try the first order exponential decay function

$$y = y_0 + A_1 e^{-\frac{x}{t_1}}, \qquad (5)$$

where y_0 , A_1 and t_1 are fitting parameters. t_1 relate to a temperature threshold. The second one , we utilize the Gompertz function

$$y = ae^{-\exp(-k(x-x_c))}, \quad (6)$$

which is the exponential of exponential function ,so it is more complicate than the former. Here a, k and x_c are fitting parameters. To simplify (6) one may do a Taylor expand of the Gompertz function, the first two term are the first order exponential decay, $y = a(1-\exp(-k(x-xc)) + \frac{\exp(-2k(x-xc))}{2!} + \ldots$. it should be noted the Gompertz usually used to analyze the dynamic growth of biological system such as tumor growth. From the data fitting of the equation (5) ,we got $y_0 = 0.49086 \pm 0.00587$, $A_1 = -1.07167 \pm 0.06719$, $t_1 = 0.57345 \pm 0.0334$ with the regression R^2 = 0.99072 and $Chi^2 = 0.00018$ as shown in figure 8. For the function in (6) ,it give $a = 0.47887 \pm 0.00178$, $x_c = 0.74876 \pm 0.00572$, $k = 2.93334 \pm 0.06797$,with the regression R^2 = 0.9987 and $Chi^2 = 0.00002$ as shown in figure 8.From R^2 and Chi^2, it is shown that the Gompertz function[24] might be more suitable a function to be fit our data.

For not very low temperature like $T \geq 3.5T_c$ this findings might not be evidently clear because one could argue that it could be the correction to the dynamic scaling that cause that deviation. However, after extensively simulations we are convinced that those can not be the same universality classed because of such great deviation from the slope 0.5. One explanation may be the following. For the case of the random walk] and biased walk, the nature corresponding to the random walk is dominated that is the no-feed back effect due to the local and change of the nearby environment comes to play. The walker recklessly wanders through the system regardless of the change of the environment landscape. In contrast, for the finite temperature case the non linear feed-back crucially comes to play and dramatically changes the nature of the walker to become much more active walker. Now, the changes of the landscape or energy or barrier caused the nonlinearly feed-back to how it walk for the next step. The affect is highly non-linear even though it still controlled by the driving force to evolve the system to the “appropriate” steady state. As the temperature decrease, the particle become more and more correlated resulting the extinct of the random walk nature which is driven by the uncorrelated thermal fluctuation. We have plot the relation between the slope and the temperature as shown in the fig. 7 and fig.8.

With the significant change of the slope, we now believe that the scaling law for the highly active walk corresponding to the moderate and low temperature should be different from that of in high temperature or bias walk case. Their universality classes are arguably not the same. In the case of lower temperature, even the microscopic dynamics is local, due to the interaction between the particle the correlation is now dominated. As seen even from the snap shots, the correlation length, $\xi(T)$ depends on the temperature. Well known, as T approaches T_c, $\xi(T)$ tends to $O(L)$ and no characteristic length scale as in the critical phenomena. Therefore, the short length, no memory impact of random walk is broken down. In our simulations, one can notice the $\xi(T)$ in units of the lattice spacing.

3.3. Time-dependent structure factors.

We focus on the SFs whose wave vectors perpendicular to the initial interfacial boundary where nx =0 and ny =/ 0. To compromise the computer run time, we will give the results only ny from 1 to 6. The rest is expected to give the similar features as the first sixs without any dramatic change. We shall refer as the odd and even wave vector index. Of course, from definition of SFs, S(t=0) is of order L^2 when ny is odd and is the order $(L^2)^{-1}$ when ny is even. This would be another way around if we instead use the odd lattice size. Since we will only consider the T> Tc so that the equilibrium configuration is homogeneous . Therefore, S(t-> infinity,and T>>1) = 1 for both odd and even wave vectors.

For reference, we briefly review a few results from[25]. There they focus on the infinite temperature case. As in the previous section, three regimes emerge once again namely early(E), intermediate(I) and saturation(S) regimes , separated by two characteristic times. It starts of with the E regime until the time is the order of L^2 marking the onset of I regime. In I regime, the odd SFs are governed by the exponential decay function. In contrast, even SFs behave like the power law with the slope unity and then develop surprising “dip”s before they finally reach equilibrium equal unity with the slope about 0.5 as shown in the graph.

Turning to the finite temperature, due to two characteristic time scale of vacancy and the bulk inter-diffusion of binary alloys, the three regimes still persist. Of course the marking time scale are longer than the infinite temperature case because now the correlation is much more complicate. Also the dips seen before are still present. However, The portion of the graph giving the scaling exponent of slope = 1 in the I regime now is getting more taken over by the slope = 0.5. This is clearly seen when the wave vectors are small but somewhat obscured when wave vectors are large. This suggests that highly correlation due to the finite temperature could break the universality of the scaling of infinite temperature. This is of course is caused by the microscopic mechanism of how vacancy move and non-linearly interacts with the environment. This is not yet fully understood and yet to be seen.

4. Summary and Conclusion

We investigated the vacancy-driven disordering process of an initially phase segregated binary system. To compare with a base-line study for the case following the upquench from T=0 to T= inf, we consider upquenches to finite temperature T< inf. Performing MC simulations for the range of temperatures, we seek to establish whether the scaling exponents of the Brownian vacancy case remain valid. Qualitatively, we monitored the change of the configurations as time goes on by taking snapshot sequences. Quantitatively, we measure the time-dependent disorder parameter A(L,T;t) and structure factors(S).

From the numerical data analysis of the slope of A(L,T;t) vs. t, we found that the these scaling exponent no longer holds especially for low T. This is due to inter-particle interaction now play a role, correlation in the system switches from the short-range so that the vacancy does not perform a random walk. We purpose the fitting function of the slope versus temperature using exponential and Gompertz function. The later seems to be the better fit.

For the time-dependent structure factor, in comparison with the infinite temperature case, we observe that for not equal 1 and the slope =1 is obscured and finally disappear for so low temperature.

Even though this model is simple, it forms the basis for description of a large variety of related systems.

Acknowledgements

This research is supported in part by Thai Research Fund through the grant number TRG4580090 and RTA4580005 and MTEC Young Research Group funding MT-NS-45-POL-14-06-G. The Royal Golden Jubilee Ph.D. Program (PHD/0240/2545) to Jirasak Wong-ekkabut and I-Ming Tang is acknowledged.

References

1. H-F. Meng and E.D.G. Cohen, Phys. Rev. E51, 3417 (1995);

2. J. Krug and P. Meakin, Phys. Rev. Lett. 66, 703 (1991);

3. R. Cuerno, H.A. Makse, S. Tomassone, S. Harrington and H.E. Stanley, Phys. Rev. Lett. 75, 4464 (1995)

4. D. Drouin, J. Beauvais, R. Lemire, E. Lavall'ee, R. Gauvin, and M. Caron, Appl. Phys. Lett. 70, 3020 (1997).

5. P.J. Shah and O.G. Mouritsen, Phys. Rev. B41, 7003 (1990);

6. W.D. Callister Jr., *Material Science and Engineering: An Introduction* (Wiley, 1994).

7. B.M. McCoy and T.T. Wu, *The Two-Dimensional Ising Model* (Harvard University Press, 1973).

8. A. J. Bray, Adv. Phys. 43, 357 (1994).

9. O.G. Mouritsen and P.J. Shah, Phys. Rev. B40, 11445 (1989);

10. P.J. Shah and O.G. Mouritsen, Phys. Rev. B41, 7003 (1990);

11. E. Vives and A. Planes, Phys. Rev. Lett. 68, 812 (1992)

12. K. Yaldram and K. Binder, Acta metall. mater. 39, 707 (1991),

13. K. Yaldram, G.K. Khalil and A. Sadiq, Solid State Comm. 87, 1045 (1993);

14. P. Fratzl and O. Penrose, Phys. Rev. B50, 3477 (1994)

15. S. Puri, Phys. Rev. E55, 1752 (1997);

16. S. Puri and R. Sharma, Phys. Rev. E57, 1873 (1998).

17. B. D. Hughes, *Random Walks and Random Environments},*
Vol. 1:it Random Walks (Clarendon Press, Oxford, 1995).}

18. Master equation

19. L. Onsager, Phys. Rev. 65, 117 (1944).

20. N. Metropolis, A.W. Rosenbluth, M.M. Rosenbluth, A.H. Teller, and E. Teller, J. Chem. Phys. 21, 1087 (1953).

21. Z. Toroczkai, G. Korniss, B. Schmittmann and R. K. P. Zia, Europhys. Lett. 40, 281 (1997).

22. B. Schmittmann, R.K.P. Zia, and W. Triampo, Braz.. J. Phys. 30, 139 (2000)

23.W. Triampo, T. Aspelmeier, and B. Schmittman, Phys. Rev. E61. 87, 2386(2000)

24. Gomperz function

25. T. Aspelmeier, B. Schmittman, and R.K.P. Zia, Phys. Rev. Lett. 87, 065701-1 (2001)

Effects of static magnetic fields on the growth of leptospire, *Leptospira interrogans serovar canicola*: Immunological reactivity and cell division

Wannapong Triampo[1,4*], Galayanee Doungchawee[2], Darapond Triampo[3], Jirasak Wong-ekkabut[1], and I-Ming Tang[1,4]

[1]Department of Physics, Faculty of Science, Mahidol University, Bangkok 10400, Thailand

[2]Department of Pathobiology, Faculty of Science, Mahidol University, Bangkok 10400, Thailand

[3]Department of Chemistry, Faculty of Science, Mahidol University, Bangkok 10400, Thailand

[4]Capability Building Unit in Nanoscience and Nanotechnology, Faculty of Science, Mahidol University, Bangkok 10400, Thailand

*Corresponding author, E-mail: scwtr@mahidol.ac.th and wtriampo@yahoo.com

Abstract: The effects of exposure of Leptospira bacteria, *L. interrogans* serovar *canicola* to a constant magnetic field with magnetic flux density from permanent ferrite magnet = 140±5 mT are studied. Changes in the leptospira after their exposure to the field were determined by changes in their growth behavior and agglutination reactivity with homologous antiserum using dark field microscopy together with visual imaging. The data showed that the exposed leptospira have cell densities and agglutination reactivity lower than those for an unexposed control group. Interestingly, some of the exposed leptospira were observed to be abnormal in their morphology, e.g., their cells were longer in length. We discussed some of the possible reasons for our observations.

Key words: Leptospirosis, *Leptospira interogans*, Magnetic field, dark field microscopy, immunological reactivity, cell division

I. INTRODUCTION

Leptospirosis is an acute febrile illness caused by pathogenic spirochete bacteria of genus *Leptospira* [1,2]. This disease has emerged as an important public health problem worldwide. The illness resulting from this disease can range from being a mild flu-like illness to being a severe (often fatal) disease involving renal and/or liver failure and hemorrhage (referred to as Weil's syndrome) [3]. Most outbreaks tend to be seasonal in nature and are often linked to environment factors, to animals and to agricultural and occupational cycles like cultivating rice in marshy land . Mammals such as rats and cattle are commonly involved in the transmission of this disease to human via direct or indirect exposure to contaminated tissues or urine[1, 2,4]. Out-breaks of leptospirosis occur mainly after flooding, leading it to becoming an occupational hazard for sanitary and agricultural workers as well as a recreational hazard for humans [5]. Some pathogenic leptospira have also been found to be associated with domesticated animals. For example, serovar canicola (*L. canicola*) has adapted itself to canines and so it has become common in many human communities. Although there has been no report of leptospirosis in the canines living in Thailand, there is a great potential for transmission of the disease between human and dogs kept as household pets, unless one is aware of the disease.

L. canicola bacteria used in our study are motile aerobes that are very thin, flexible and spiral-shape about 0.1 μm wide and 6-20 μm long. Leptospira are difficult to see with a light microscope. They can, however, be seen by a dark field microscopy of a wet sample. This allows for the agglutination reactivity to be determined. The leptospiral outer membrane or surface antigens can be detected through its agglutination with the homologous anti-serum. The optimal conditions for its growth and as well, its biology are well documented in the literature[1,2]. Moist environments with a neutral pH provide suitable conditions for survival of leptospira outside the host. The cultivating temperature is approximately 20-32°C. In general, leptospira are highly susceptible to adverse environmental conditions such as exposure to drying, to chemicals like detergent chlorine or iodine, to unfavorable pH(> 8.0 or < 6.5), to strong electromagnetic fields and to high temperatures (above 40°C).

Magnetic fields (MF) also affect various biological functions of living organisms, e.g., DNA synthesis and transcription [6], as well as ions transportation through cell membranes [7]. Almost all living organism experience magnetic fields arising from one or another source. The geomagnetic field on the surface of the earth is approximately

0.50-0.75 gauss in strength. There have been several studies on the effects of exposure to the magnetic field and several of these have given rise to controversies over the past decades. The growth rate of the Burgundy wine yeast has been shown to decrease when an extremely low magnetic flux density (MFD) of 4 gauss is applied [8]. The growth of *Trichomonas vaginalis* is accelerated when it is exposed to 460-1200 gauss [9]. The growth of *Bacillus subtilis* increases when exposed to 150 gauss and decreases when exposed to more than 300 gauss [10]. Similar results are reported for *Chlorella*, an exposure of less than 400 gauss increases the growth, while exposure to 580 gauss decreases the growth [11]. Most studies point to the magnetic field influencing the growth and survival of the living organisms differently at different MFD [12, 13, 14, 15]. Other researchers have studied the effects of the magnetic fields on the bacteria at the enzyme level [16] or at the genetic level [17].

To study the efficacy of using magnetic field to control or prevent the growth of leptospira, we have applied magnetic field(MF) on selected leptospira at various intensity relying on the exposure duration levels. We have then determined the agglutinating activity of the experimental bacteria using dark field microscopy.

II. MATERIALS AND METHODS

Pathogenic Leptospira intetrrogans, serovar canicalo was selected for this study. The bacteria was grown in an EMJH liquid medium using the method of Ellinghausen and McCullough, as modified by Johnson and Harris [2]. The bacteria were grown at a temperature 27±1°C in the dark.

Permanent ferrite magnet of cylindrical shape with 5 cm. in diameter was placed beside the 15 ml culture glass tube(less than millimeter apart but not touched) containing 1 ml of cell suspension of newly sub-cultured leptospires in EMJH liquid medium. Field magnitude and homogeneity of 140 ± 5 mT(north pole) were checked by means of a TESLAMETER(Hall effect Teslameter digital, Order No. 13610.93 , Phywe Systeme GMBH, 37070 Gottingen Germany). The choice of the intensity of the static magnetic field in our experiments was made roughly according to the report by Genkov et al., 1974 in which this intensity was indicated by the authors as the intensity from the constant magnetic field to induce the growth and development of *Trichomanas vaginalis*. and availability of the magnet. For this type of exposure, no shielding against the natural variations of terrestrial MF was required, their values (ranging at approx. 0.050 mT) being negligible with respect to the MF intensities applied. It should be

emphasized that simultaneous experiments by omitting the magnet were performed as control which was placed at the distance about 1 meter from the exposed group.

In the absence of the magnets, the MFD was 0.05±0.01 mT. All bacterial samples were placed in the MF under different time durations of MF exposure, i.e., 0 day(control sample), 1, 2, 3,4,5 and 6 days. After MF treatment individual samples were further incubated until 7 days of experimentation. Immediately after day 7 of incubation, all samples were observed under a dark field microscope(due to the property of cell's develop) and pictures were the collected by CCD snap shots for the growth and agglutination properties using the microscopic agglutination technique (MAT) with homologous antiserum and scored for reactivity as follows

4+ = 100 % clearance of leptospires from the field
3+ = 75 % clearance of leptospires from the field
2+ = 50% clearance of leptospires from the field
1+ = 25% clearance of leptospires from the field

This MAT test has been typically used as a diagnostic tool for leptospirosis. This may not be the most reliable measure, it however arguably is the most appropriate technique for this study. With the same set of conditions and specimens the experiment was repeated twice.

AFM methodology and sample preparation

The Scanning Probe Microscopy (SPM) (Digital Instruments Veeco Metrology Group, New York) was used for AFM surface morphology imaging. The image was acquired in contact mode showing height contours that highlight the spiral shape and fine surface morphology. AFM scanner with hardware correction for non-linearities of the piezoelectric element was used. The scanner has a maximum xy range of 125 by 125 μm and z range of 6 μm. Cantilevers of Si_3N_4, 125 μm long and 35 μm wide with spring constant of 0.58 Nm^{-1} were used. In order to locate the area of interest on the samples and identify any bacteria, we used the built-in long-range on axis microscope, capable of a 5:1 zoom and x 3,500 magnification. Imaging was used at scan speeds of between 1 and 50 $\mu m / s$. The image was acquired at 256x256 pixels and was

processes by SOFTWARE. A typical imaging session began by using the built-in optical microscope and moving the x-y table in the search for bacteria. The AFM cantilever was then moved forward the surface in the proximity of the chosen bacterium.

Each sample was prepared using the method described above. In addition, it was dropped on a microscope glass slide and simply dried in air.

III. RESULTS AND DISSCUSSION

In Fig. 1, we see the atomic force micrograph (AFM) of a *L.interrogans serovar canicola* bacteria taken with a Digital Instrument Nanoscope IIIa in the contact mode. The picture shows the normal morphology of *L. interrogans serovar canicola ,* i.e., the spiral structure of leptospira. It is worth noting that the AFM usually reveals the actual roughness of the surface of the bacteria envelope. Other types of microscopy frequently show the surface to be relatively smooth. This technique was also used to see the surface morphology of the bacteria before and after the exposures to MF. It should be noted that our picture is not very clear as we wanted to, so that it does not demonstrate a “rough” envelope very clear. However, it did show the normal bacterial morphology.

Fig. 2 shows some representative dark-field micrographs of *L. interrogans serovar canicola* taken at logarithmic growth phase (at 1:10 dilution culture samples) under different time durations of MF exposure, i.e., of 0 days, 2 days, 3 days and 6 days. After 7 days of incubation, every sample tested were observed under a dark field microscope and pictures were the collected by CCD snap shots. Even though there were some noises in the images, the decrease of cell growth could be seen by visual observation. The implications of these observations are not insignificant given the results of the other studies[6-17]. From the Fig. 2A to 2D, one can clearly see that the cell density decreased as the exposed time increased, especially, when more than 3 days. This shows the decrease in the growth resulting in the decrease of the number of bacteria. This is one of the factors that is lower the degree of agglutination due to few number of living bacteria left to agglutinate.

In Fig. 3, the dark-field micrographs of agglutinated bacteria after reacting with the specific antiserum, showing complete agglutination (100% reactivity) Fig 3A., and 50% agglutination (with only half of free living bacteria present) Fig. 3B.,Based on criteria mentioned at the end of the previous section, the agglutination reactivities of the *L. interrogans serovar canicola* subjected to different levels of MF exposure are

listed in Table I (at higher exposure time, the leptospiral bacteria were demonstrable with a lower agglutination level against the reference antiserum tested. The end point of reactivity is noted and scored as 50% agglutination (2+)). The agglutination scoring decline with the longer explosure treatment of the lectospires as shown in Fig.4. Comparing the MAT results of the control leptospires (0 day exposure) and those of the bacteria after exposure to the MF, we found that the latter groups (particularly those of the longer exposure) express lower levels of agglutination reactivity. These findings might reflect the presence of a lesser amount of agglutinin or number (density of the leptospires) than those in the control samples. It should be emphasized that with the same set of conditions and specimens the experiment was repeated twice and they gave exactly the same (semi-quantitative) results. From the data of scoring, it therefore did not show the error. Once again, each experiment set, it has 1 control(non-exposed) group and 6 exposed groups with different duration of exposure times

Besides the cause of the decrease in the degree of agglutination as mentioned above which is due to the decrease in the number of leptospira, the “denaturing effect” of antigen-antibody reaction might be speculatively the other contribution to this phenomena which can be explained as follows. Typically, the antibodies are large soluble protein molecules known as immunoglobins and are produced by B-cells. They bind to a specific antigens in a lock-and-key fashion (lock = antibody; key = antigen) [18]. Its shape should therefore be specific to a particular antigen. When the specific antibody encounters the antigen, it will form an antigen-antibody complex through some non-covalent forces such as the electrostatic force, the hydrogen bond, the van der Waal force or a hydrophobic force. When a change of a single atom occurs, the complex can lose its binding. This “specificity” is what could be the key for denaturing of the antigen-antibody reaction. Under the circumstances used in the study, the motion or transfer of any electrons or ions onto the cell membrane could induce an electric current. This current might perturb the other charge particle motion in the cell thus resulting in the loss of binding [19].

Surprisingly, we see among the leptospira exposed for 3 or more days some bacteria that are longer in length than the control bacteria (See Fig. 5). This preliminary finding probably indicates that there is some disturbance to the cell division. More experiments must be done to investigate these phenomena in order to determine the exact mechanism responsible for the observed behavior. Our present explanation for this abnormality in the cell division is based on the following: Like most bacteria and

archea, leptospira divide symmetrically possibly via the formation of a septum in the middle of the cell (since in our view, binary fission is less likely). For the time being, AFM technique is being used by us to investigate the division-related morphology. Recent evidence indicates that the protein synthesis dedicated to the process of cell division is assembled between segregated chromosomes at the proper time [20]. The key to this assembly is *Fts*Z, termed for filamentous temperature sensitive (a structural) analogue of tubulin [21]. With the DNA damage caused by MF induces mutation, this results in the abnormal synthesis of *FtsZ* which in turn could interfere or stop the cell division. Like previous studies with *E. coli*, *FtsZ* appears to induce the earliest (known) step in the cell division process. Conditional mutants of *ftsZ* in *E. coli* cause the cell not to divide. This leads to long filamentous cells that can replicate and segregate their chromosomes[22].

IV. CONCLUSIONS AND PERSPECTIVE

Looking at micrographs of *L.interrogans serovar canicola* exposed to the magnetic fields (140 mT for 1-6 days duration), we see the agglutination reactivity of the treated leptospires decrease. The longer the exposure, the greater the deterioration of leptospires. This suggests that MF affects the growth of bacteria.

The interpretation of the decrease in the agglutination level was not conclusive that this may be either due to the denaturing of the antigent-antibody active sites or the proliferation of the organism that may be involved. According to the direct observation and image snap it leads us to believe that this primarily is due to the latter cause. However, as far as we are concerned the first cause may also contribute to the degree of agglutination, even we do not know for sure how so far. Our speculation on this observation rests on reasonable fact of physical properties of how magnetic field can affect the system. It has yet to be seen what more evident resting on the basis from more experiments will give us more insight into this problem. We also observed that some leptospires became abnormally long after four days exposure to MF. This could suggest that MF may influence cell division. The mechanism of the negative effect of magnetic field on *L.interrogans serovar canicola* cannot be determined from the present experiment. The biological effect of MF might be due to its effect on the membrane permeability of ionic channels. Another possibility might be the changes induced in the DNA structure by the MF. Further investigation is needed to gain insights into the interaction of the MF with the biological systems in the leptospiral bacteria.

The benefit of our finding is at least the first step toward to the more finding and studies of this bacteria and leptospirosis. We hope with more studies and a variety of aspects of research concerning leptospirosis, it will lead to the best solution to the diagnostics, treatment and prevention scheme for this disease in the near future.

Acknowledgements

This research is supported in part by Thailand Research Fund through the grant number TRG4580090 and RTA4580005 and MTEC Young Research Group funding MT-NS-45-POL-14-06-G. The Royal Golden Jubilee Ph.D. Program (PHD/0240/2545) to Jirasak Wong-ekkabut and I-Ming Tang is acknowledged.

References

1. **Faine, S. ed.:** Guideline for control of leptospirosis. Geneva: World Health Organization, Offset Publication**. 67**,(1982).
2. **Faine, S., B. Adler, C. Bolin, and P. Perolat.:** Leptospira and Leptospirosis, Medisci, Melbourne,(1999).
3. **Sherris, J. C.:** An introduction to infectious disease. New York, Elsevier Science. (1984).
4. **Turner, L. H.:** Leptospirosis I. Trans R Soc Trop Med Hyg. **61**: 842-855. (1967).
5. American Public Health Association.: **Leptospirosis. In:Benenson, A.S. (Ed), Control of Communicable diseases Manual. American Public Health Association, Washington, DC, 293-296. (2000).**
6. Phillips, J. L., W. Haggren, W. J. Thomas, T. Ishida-Jones, W. R. Adey.: **Magnetic field-induced changes in specific gene transcription, Biochim. Biophys. Acta.** 112**: 140-144. (1992).**
7. Liburdy, R. P., D. E. Callahan, J. Harland, E. Dunham, T.R. Sloma, P. Yaswen.: **Experimental evidence for 60 Hz magnetic fields operating through the signal transduction cascade: Effects on calcium influx and c-MYC mRNA induction , FEBS. Lett.** 334**: 301-308 (1993).**
8. **Kimball, G. K.:** The growth of yeast in a magnetic field. J. Bact. **35**: 109-122 (1938).

9. **Genkov, D., A. Cvetkova, and P. Atmadzov.:** The effect of the constant magnetic field upon the growth and development of *T. Vaginallis*. Folia Medica. **16**: 95-99 (1974).

10. **Moore, R. L.:** Biological effects of magnetic fields: studies with microorganisms. Can. J. Microbiol. **25**: 1145-1151(1979).

11. **Takahashi, F., and T. Kamezaki.:** Effect of magnetism of growth of Chlorella. Hakkokogaku. **63**: 71-74(1985).

12. **Yamaoka, Y., O. Takimura, H. Fuse, and K. Kamimura.:** Effect of magnetism on growth of *Dunaliella salina*. Research in Photosynthesis **3**: 87-90(1992).

13. **Singh, S. S., S. P. Tiwari , J. Abraham, S. Rai, and A. K. Rai.:** Magnetobiological effects on a cyanobacterium, *Anabena doliolum.* Electro-and Magnetobiology. **13**: 227-235(1994).

14. **Tsuchiya, K., K. Nakamura, K. Okuno, T. Ano, and M. Shoda.:** Effect of homogeneous and inhomogeneous high magnetic fields on the growth of *Escherichia coli*. J. Ferment. Bioeng. **81**: 343-346(1996).

15. **Piatti, E., M. C. Albertini, W. Baffone, D. Fraternale, B. Citterio, M. P. Piacentini, M. Dacha, F. Vetrano, and A. Accorsi.:** Antibacterial effect of a magnetic field on *Serratia marcescens* and related virulence to *Hordeum vulgare* and *Rubus fruticosus* callus cells. Comparative Biochemistry and Physiology Part B. **132** :359-365(2002).

16. **Utsunomiya, T., Y. Yamane, M. Watanbe, and K. Sasaki.:** Stimulation of Porphyrin Production by Application of an External Magnetic field to a Photosynthetic Bacteria, *Rhodobacter sphaeroides.* J. Biosci. Bioeng. **95**: 401-404(2003).

17. **Horiuchi, S., Y. Ishizaki, K. Okuno, T. Ano, and M. Shoda.:** Drastic high magnetic field effect on suppression of *Escherichia coli* death. Bioelectrochemistry. **53**: 149-153(2001).

18. **Boyd, R. F.:** Basic Medical Microbiology, 5th edition, Little, Brown and company, (1995).

19. **Jackson, J. D.:** Classical Electrodynamics 3rd edition ,Wiley Text Books (1998).

20. **Rothfield, L., S. Justice, and J. Garcia-Lara.:** Bacteria cell division. Annu. Rev. Genet. **33**: 423-448(1999).

21. **Lutkenhaus, J.:** Ftsz ring in bacterial cytokinesis. Mol. Microbiol. **9**: 403-410 (1993).

22. **Hale, C. A. and P. A. J. de Boer.:** Direct binding of FtsZ to ZipA, an essential component of the septal ring structure that mediates cell division in E. coli. Cell **88**: 175-185(1997).